INSTITUTE OF PHYSICS PUBLISHING JOURNAL OF PHYSICS D: APPLIED PHYSICS

J. Phys. D: Appl. Phys. **34** (2001) 2109–2116 PII: S0022-3727(01)22917-9

Rutherford backscattering analysis of thin films and superlattices with roughness

N P Barradas

Instituto Tecnológico e Nuclear, EN 10, Apartado 21, 2686-953 Sacavém, Portugal and Centro de Física Nuclear da Universidade de Lisboa, Av Prof Gama Pinto 2, 1699 Lisboa Codex, Portugal

E-mail: nunoni@itn.pt

Received 6 March 2001
Published 4 July 2001
Online at stacks.iop.org/JPhysD/34/2109

Abstract

Knowledge on the thickness, composition, and interfaces of thin films and multilayers is, in many systems, fundamental for the understanding and optimization of their properties. One of the techniques often applied to such studies is Rutherford backscattering (RBS). However, it has been very difficult to account for the effects of interface roughness in the data obtained, and the alternative has been to develop dedicated data analysis codes for particular problems where roughness plays a determinant role. In this work, the effect of roughness is taken into account in the data analysis by calculating the effect of roughness on the apparent energy resolution as a function of depth. This depends on the exact type of roughness, and three different models have been implemented: inhomogeneous layer thickness, corrugated sample, and rough substrate surface. Interfacial mixing in multilayers can also be analysed with the method developed. Automatic fits to the data can be performed in this way, where the roughness parameters are derived during the fit, providing a new tool for RBS analysis. The code is applied to several systems in order to test its validity and applicability. Systems which are hard to analyse by RBS have been chosen: $Si/VS/Si_{0.65}Ge_{0.35}$ 300 nm/$Si_{0.2}Ge_{0.8}$ 4 nm/$Si_{0.65}Ge_{0.35}$ 15 nm/Si 3 nm thin films, where VS stands for a linearly composition-graded virtual substrate; and MgO/(Fe 25 Å/Co 20 Å)$_{10}$ multilayers.

1. Introduction

Knowledge on the thickness, composition, and interfaces of thin films and multilayers is, in many systems, fundamental for the understanding and optimization of their properties. One of the techniques often applied to such studies is Rutherford backscattering (RBS), which belongs to the cluster of the techniques normally referred to as ion beam analysis (IBA) [1]. Analysis of perfect samples, with well defined surfaces and interfaces, has become standard practice and normally does not pose particular problems.

However, not all samples are as ideal as that. In many cases, there is interfacial mixing and roughness, as well as substrate and surface roughness. It is difficult to account for the effects of roughness in the data obtained, and several approaches have been adopted in the past. A first group of approaches is mainly experimental: the spectra of rough samples are measured and conclusions drawn from the difference relative to measured or calculated spectra from samples with smooth surfaces and/or interfaces [2, 3]. Another group of approaches has been used when roughness of the order of a few to a few tens of nanometres are present, and consists in developing ad hoc procedures for particular given systems [4–7]. This can be a very successful procedure, but it is not general and normally requires a great deal of work.

Finally, several papers have been dedicated to developing code that can be of general use for analysing samples with surface roughness of some tens or hundreds of nanometres, but normally on the few micrometre scale [8–14], for both RBS and elastic recoil detection analysis (ERDA). While the older codes tend to make some severe approximations (such as considering only single-elemental, mono-isotopic targets), some of the more recent ones can be very sophisticated and reproduce experimental data very well. However, they involve

calculating, for a given surface, the trajectory of many ions (normally around 100, but up to several thousand) with the entrance and exit at different points of the surface, and then averaging the result.

This process requires a good knowledge of the nature of the surface to be investigated. It is also slow and cumbersome, even with modern computers, if one considers that in analysis of real data one must evaluate many functions until a good simulation is obtained. Finally, these codes are applicable to the case of surface roughness only, and so far the codes reported cannot analyse interfacial roughness. Nevertheless, they work excellently for the purpose for which they have been developed.

In this work a completely different approach is taken, which is most appropriate for thin films and multilayers with roughness values up to a few tens or hundreds of nanometres. The effect of roughness is, in many cases, similar to that of energy straggling; that is it leads to an additional broadening of the features present in the energy spectrum. By calculating the broadening due to roughness, and assigning it as an extra contribution to the energy straggling, an apparent energy resolution is obtained. This can then be convoluted with the theoretical spectrum in the normal way. The effect of roughness can thus be included in a standard code with little effort, paying only a small price in terms of calculation time.

The broadening depends on the exact type of roughness, and three different models have been implemented: inhomogeneous layer thickness, corrugated sample, and rough substrate surface. Interfacial mixing in multilayers can also be analysed with the method developed. These models have been introduced in the well known code IBA DataFurnace, which has previously been developed to analyse RBS, ERDA, non-resonant nuclear reaction analysis (NRA) and neutron depth profiling (NDP) data [15–17]. It can perform automatic fits to several spectra collected from the same sample, ensuring all the information in the data is used to obtain the final answer, such as a depth profile or the roughness parameters. It can also generate theoretical spectra for given parameters.

The code is applied to several systems in order to test its validity and applicability. Systems which are hard to analyse by RBS have been chosen: $Si/VS/Si_{0.65}Ge_{0.35}300nm/Si_{0.2}Ge_{0.8}$ 4 nm/$Si_{0.65}Ge_{0.35}$ 15 nm /Si 3 nm thin films, where VS stands for a linearly composition-graded virtual substrate; and $MgO/(Fe\ 25\ Å/Co\ 20\ Å)_{10}$ multilayers. The results are excellent, providing a new tool for RBS analysis.

2. Experimental details

The RBS analysis was performed using a 1.0 or 1.6 MeV He^+ beam. A surface barrier detector located under the beam at 160° to the beam direction (Cornell geometry) was used. The 15 keV energy resolution of the system was determined from the signal of thin Au and Ni layers. For each sample, spectra were collected at different angles of incidence, that is the tilt angle ϑ, defined as the angle between the beam direction and the sample surface. The beam was between 0.2 and 0.6 mm wide (the value was different in different experiments, normally wider for normal incidence and narrower at grazing angle of incidence) and 0.6 mm high. The detector aperture was either circular with 3 mm diameter or 1.5×5.0 mm^2 to reduce the angular dispersion of the backscattered beam. The detector–sample distance was 75 mm. The 5 nA beam current was measured with a transmission Faraday cup with precision around 2% [18]. The pressure in the target chamber during the experiments was around 10^{-7} mbar.

3. Roughness models and energy resolution as a function of depth

3.1. Energy straggling

In RBS analysis the energy resolution degrades with depth, and faster at grazing angles of incidence. The result is an artificial broadening of any interface signal in the spectra obtained, and also a distortion of the spectral shape relative to what it would be if the resolution were constant with depth. This distortion is, in a bulk sample, an increased yield at low energies.

Any interface studies with RBS (or other IBA techniques) must take energy straggling into account as precisely as possible or the results will be an artefact. In particular, any values obtained for roughness will be much larger than the true ones. The reason is that one apparent effect of roughness at a given depth is that of increased energy resolution at that depth. If the energy resolution is under-estimated, the roughness will be over-estimated. To obtain realistic roughness parameters the effect of energy resolution degradation must therefore be taken into account.

We have implemented both Bohr and Chu energy straggling with effective charge scaling according to the algorithms given in [1, 19]. However, this does not take into account the influence of other effects, such as geometrical dispersion caused by the finite beam size and by the detector's solid angle, and plural and multiple scattering, and may be unrealistic when those effects are predominant, as in grazing angle of incidence experiments normally performed for very thin films and multilayers.

The computer code DEPTH [20, 21] takes all these effects into account, except for the small low-energy tails due to plural scattering. DEPTH has been validated within 10% for several systems, including Si [22], Si/Ge [23], and Co/Re [4]. Deviations up to 30% have been observed for heavy ion ERDA using a 154 MeV ^{197}Au beam on Al and Co thin films [6]. Our code can use, in the automatic fits it performs, the resolution as calculated with DEPTH, ensuring that the results obtained are as realistic as the current state of the art permits.

3.2. Roughness models

The next step is then to develop different roughness models, corresponding to different physical situations, and implement them in terms of what the effect in the broadening of any spectral feature is. In other words, one tries to define the effect of roughness on the apparent energy resolution as a function of depth. We have previously developed three models of roughness, which may approximate real physical situations [4]. In all of them it was supposed that the contribution to the depth resolution caused by the surface roughness follows a Gaussian distribution, is independent from the other contributions, and can be added to them in quadrature. The models are as follows.

(1) The roughness is caused by the inhomogeneity in the layers thicknesses (refer to figure 4(a) of [4]). This will always be present to some extent if the thickness of a layer is not an exact multiple of the thickness of one atomic layer. It can also be due to processes such as islanding during growth. Assuming that the contributions of each layer are independent of each other, then the total contribution, δX_n^{inh}, to the broadening at the interface between the nth layer and the following one is

$$\delta X_n^{inh} = \sqrt{\sum_{i=1}^{n} (\delta X_i)^2} \tag{1}$$

where δX_i is the inhomogeneity of the ith layer (counting from the surface). The quantity δX_n^{inh} is the standard deviation of a real thickness. One should note, however, that RBS is sensitive only to areal densities, and δX_n^{inh} can be given directly in some areal density unit such as the commonly used 10^{15} at cm^{-2}. It is then converted into an energy resolution (standard deviation) value by using the stopping cross section factor $[\varepsilon]$ [24, 25] and the density N of each given layer:

$$\delta E = [\varepsilon] N \delta X. \tag{2}$$

Equation (1) describes the resolution *after* the layer with inhomogeneous thickness. The question arises of what happens *in* the layer. Suppose that it is the only layer with thickness inhomogeneity. Then, at its surface (i.e. at the interface of the rough layer with the layer on top of it, i.e. closer to the sample surface) there is no broadening. The broadening will only start to be felt when the beam reaches a region where in some areas it is still inside the rough layer, and in other areas it is already in the next, deeper, layer. This will be a gradual process, and depends on the relation between the roughness and the thickness of the layer: for very thick rough layers, the effect of roughness will only be felt at the bottom. For roughness values comparable to the layer thickness, the effect is felt in the whole layer.

(2) The roughness is connected to the fact that the sample is slightly deformed or corrugated. This may happen due to stress, or if the substrate was corrugated to start with. Consequently there will be a variation $\delta\vartheta$ in the angle of incidence, which leads to a spread δp in the length p of the path the particles make to probe at a certain depth (refer to figure 4(b) of [4]). That spread will be perceived as coming from a spread in the thickness of the layers. The resulting contribution at depth X, δX^{def}, can be calculated by differentiating $X = p \cos\vartheta$, and is

$$\delta X^{def}(X, \vartheta) = X \operatorname{tg}\vartheta \, \delta\vartheta \tag{3}$$

The quantity δX^{def} is the standard deviation of a real thickness, and the exact depth dependency in equation (3) depends on the fact that X is a real thickness, not an areal density. Hence all the calculations must be made for real thickness values, and then converted into areal densities by using the density of each layer. This will introduce small discontinuities in the apparent energy resolution calculated, because the density is a discontinuous function of the structure whenever there are abrupt compositional changes. This is not an artefact, it is a real effect as long as the model is accepted as valid. However, the question arises of how to calculate the density of each layer. A simple weighted average of the elemental densities present is normally an inadequate approximation. In the code implemented, it is hence possible to introduce known densities for given molecules in the input.

(3) The roughness is connected to the surface roughness of the substrate, with all the interfaces closely following the substrate surface (refer to figure 4(c) of [4]). This will happen if the film grows uniformly on top of the surface. Consequently, when the ions enter the surface in a given point A and are backscattered at a thickness X at a different point B, the contribution will appear only if there is a lateral distance $l = X \operatorname{tg}\vartheta$ between A and B. The contribution, δX^{subst}, will increase with l until reaching a saturation value δX, which is the standard deviation of the height distribution of the substrate surface. The exact shape of this saturation behaviour depends on the shape characterizing the surface roughness (such as smooth waves, steps, sawtooth-shaped elevations, or others) and should be determined from independent measurements for the different kinds of surfaces and implemented accordingly. Lacking such detailed knowledge, it can be approximated by an error function, resulting in

$$\delta X^{subst}(X, \vartheta) = \delta X \operatorname{erf}(X \operatorname{tg}\vartheta / L) \tag{4}$$

where L is the correlation length, being of the order of magnitude of the lateral size of the surface structures. Again, δX is a real thickness value, and the results must be converted into areal densities using layer densities.

(4) Finally, suppose a multilayer where there is interfacial mixing between layers. This is not, strictly speaking, roughness. The signal from each layer will be broader than if the interfaces were abrupt. Assuming that the interfacial mixing is the same for all layers (which is common in multilayers), then the observed signal broadening will be exactly the same for all layers. This can be simulated using model (3) with a very small L value, such that the saturation value δX is reached at the depth of the first bilayer. The standard deviation δX then reflects the interfacial mixing, and the corresponding full-width at half-maximum (FWHM) can be taken as the width of the mixed interface.

3.3. Calculations: effect of roughness parameters

Models (1)–(3) were implemented in the IBA DataFurnace computer program [15]. This program performs automatic fits to multiple spectra collected from the same sample. The parameters in equations (1)–(4) are treated as free fit parameters. They are for model (1) the δX_i, for model (2) $\delta\vartheta$, and for model (3) δX and L. The code can also be used to simulate theoretical spectra for a given structure with given roughness.

We used the IBA DataFurnace program to calculate theoretical spectra for the system Si/(Si 4 nm/Ge 6 nm)$_5$, using the three different roughness models implemented. This particular system was chosen since its multilayer structure makes it easier to observe the effect of each roughness model on different parts of the spectrum corresponding to different depths. The calculations were performed for typical experimental conditions for such thin layers; that is, 1.0 MeV He^+ detected at $\vartheta = 10^\circ$.

The energy resolution as a function of depth was calculated for this system with the code DEPTH [20]. Then, the contribution to signal broadening due to a given roughness model and roughness parameters was calculated, and added in quadrature to the energy resolution as calculated with the DEPTH. The result is an apparent energy resolution that can be used to calculate an RBS energy spectrum following the usual numerical procedures [26].

This method assumes that the resolution functions involved are Gaussian shaped, which, being generally a good approximation, is not strictly true. Given the approximations already used in the calculation, both of the energy resolution and of the roughness broadening, the procedure should not add any appreciable error to the final result, which, in any case, can never be better than the energy straggling calculation, which has a 10% error as mentioned above. Finally, the apparent energy resolution values, calculated as standard deviation of the energy, were converted into the usual FWHM.

This method is not valid when the beam enters and leaves the sample more than once, as is the case when the surface has large roughness features, normally around hundreds of nanometres high, and a grazing angle of incidence is used. For this special case, and if only surface roughness is present, codes such as those reported in [11–14] can be used.

Calculations were performed using model (1), for a roughness of $\delta X = 1$ and 2 nm at the first Ge layer and for $\delta X = 2$ nm at the third Ge layer. These values are introduced as areal densities, calculated using the bulk Ge density. In all cases no other roughness was included in the calculations. The results are shown in figure 1. There is a rather abrupt step in the resolution at the layer with roughness. This is because the layer is very thin; for thicker layers, the transition would be much smoother. After the rough layer, the broadening due to roughness remains constant, and further increases in the apparent energy resolution are solely due to the energy straggling. On the other hand, if several layers have an inhomogeneous thickness, the broadening will increase after each one of them.

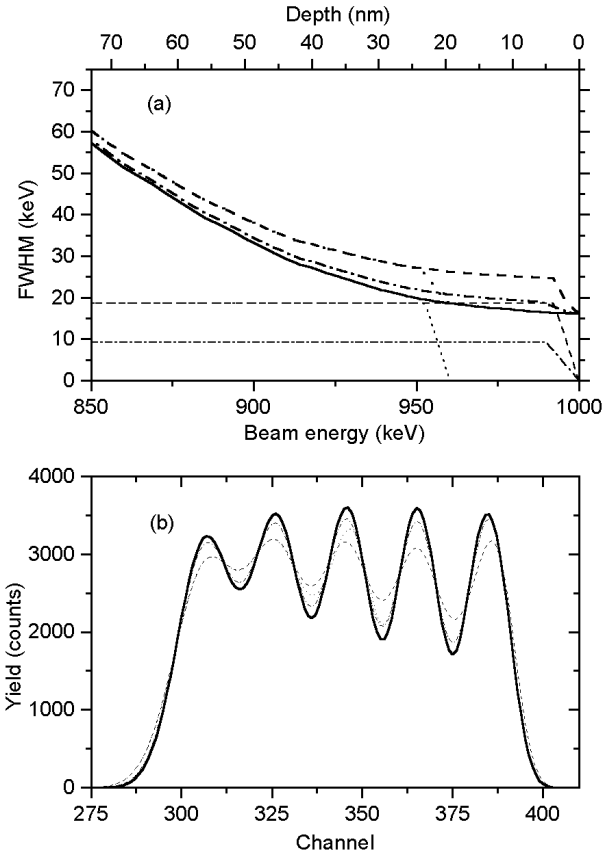

Figure 1. Calculations for system Si/(Si 4 nm/Ge 6 nm)$_5$ with roughness model (1). Full curve, results without roughness. Dashed curves, $\delta X = 2$ nm at the first Ge layer. Dashed–dotted curves, $\delta X = 1$ nm at the first Ge layer. Dotted curves, $\delta X = 2$ nm at the third Ge layer. (a) Apparent energy resolution (FWHM) for Ge. The lower curves denote the roughness contribution to the apparent energy resolution. The upper curves denote the total apparent energy resolution. (b) Corresponding theoretical spectra. Only the Ge signal is shown.

When roughness is introduced at the top, surface, Ge layer, the effect on the calculated spectra is obviously present from the very beginning (around channel 390). It is smaller for $\delta X = 1$ nm, and only for $\delta X = 2$ nm, already large compared to the 6 nm thickness of the Ge, is there observable broadening towards the surface. On the other hand, when roughness is introduced in the third Ge layer only the resulting spectrum is coincident, in the first two Ge layers (channels 360–400), with the spectrum calculated without roughness. This is so because down to the third Ge layer there is no roughness contribution to the apparent energy resolution, which then remains equal to the energy resolution. Deeper than the third Ge layer, however, the contribution to the apparent energy resolution is the same for $\delta X = 2$ nm irrespective of whether it was introduced in the first or in the third Ge layers. Hence, the corresponding spectra are coincident in the fourth and fifth Ge peaks (channels 275–330). Summarizing, the effect of model (1) roughness on the calculated spectra depends crucially on how much roughness is introduced and where.

Calculations were performed using model (2), for a variation in the angle of incidence of $\delta\vartheta = 0.5^\circ$ and $\delta\vartheta = 1^\circ$. In all cases no other roughness was included in the calculations. Note that these $\delta\vartheta$ values correspond to an apparent variation in layer thickness of $\delta X = 0.5$ and 1 nm per (Si 4 nm/Ge 6 nm) bilayer, respectively. The results obtained are shown in figure 2. The broadening due to roughness is a smooth function, increasing continuously with depth. That is, its depth dependence is completely different from that of model (1) roughness, and can be used, together with their angular dependence, to distinguish between them. The small oscillations at depths smaller than 50 nm are due to the conversion from real thickness values (nm) into areal densities (at cm^{-2}), using the Si and Ge densities in the different layers.

In model (2) there is one single parameter that determines how fast the broadening due to roughness increases with depth. For steep increases, however, this may lead to unexpected results. For instance, for $\delta\vartheta = 1^\circ$, the third and fourth Ge peaks appear slightly dislocated to lower channels, which would normally be interpreted as a larger depth. The effect is not an artefact. It is due to the rapidly increasing apparent energy resolution: for instance, it is much larger at the fourth Ge layer than at the second Ge layer, leading to more counts in the channels corresponding to depths between layers three and four (that is, to the left-hand side of the third peak) than in the channels cor-

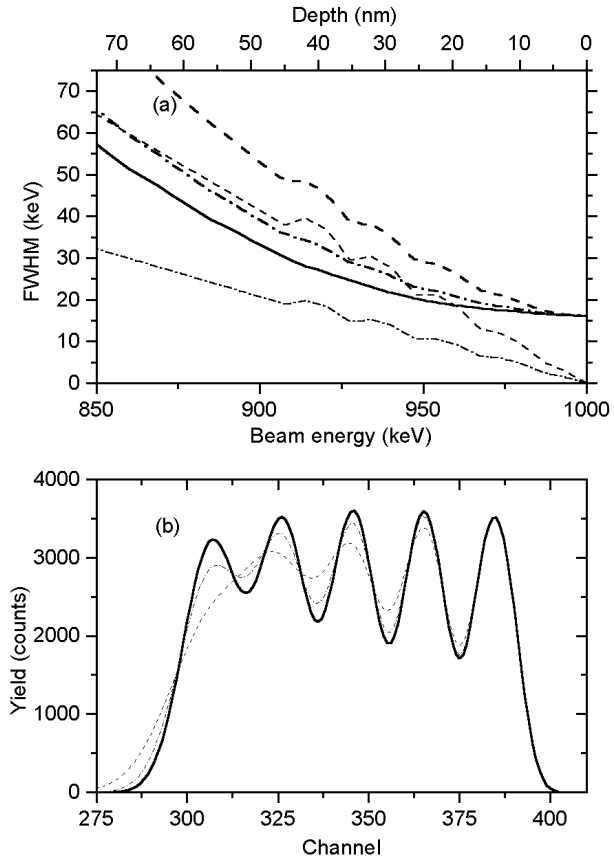

Figure 2. Calculations for system Si/(Si 4 nm/Ge 6 nm)$_5$ with roughness model (2). Full curve, results without roughness. Dashed curves, $\delta\vartheta = 1^\circ$. Dashed–dotted curves, $\delta\vartheta = 0.5^\circ$. (a) Apparent energy resolution (FWHM) for Ge. The lower curves denote the roughness contribution to the apparent energy resolution. The upper curves denote the total apparent energy resolution.
(b) Corresponding theoretical spectra. Only the Ge signal is shown.

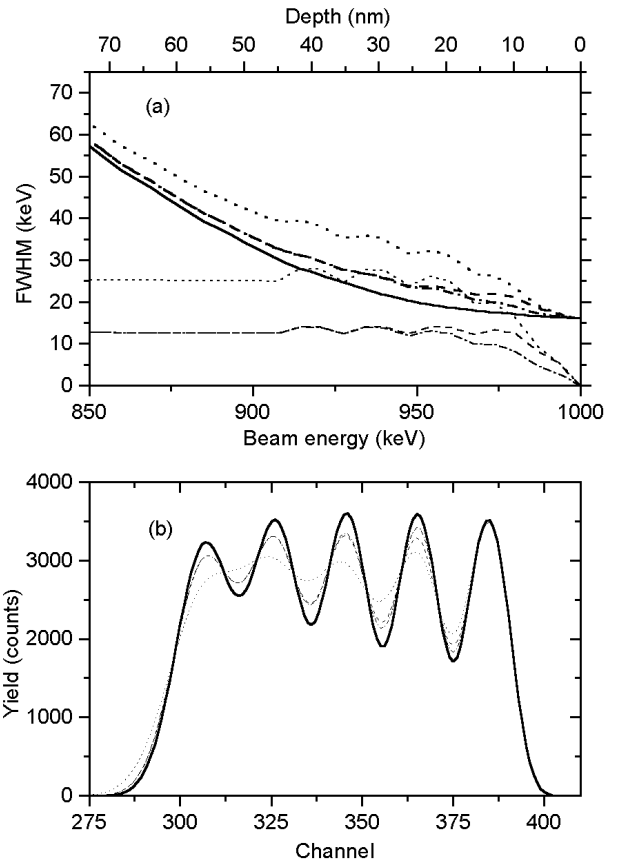

Figure 3. Calculations for system Si/(Si 4 nm/Ge 6 nm)$_5$ with roughness model (3). Full curve, results without roughness. Dashed curves, $\delta X = 1.5$ nm, $L = 50$ nm. Dashed–dotted curves, $\delta X = 1.5$ nm, $L = 100$ nm. Dotted curves, $\delta X = 3$ nm, $L = 100$ nm. (a) Apparent energy resolution (FWHM) for Ge. The lower curves denote the roughness contribution to the apparent energy resolution. The upper curves denote the total apparent energy resolution. (b) Corresponding theoretical spectra. Only the Ge signal is shown.

responding to depths between layers three and two (that is, to the right-hand side of the third peak). In this way the third peak appears dislocated to its left-hand side; that is it is apparently deeper. When this effect is not taken into account, the exact depth of each layer is incorrectly evaluated, if only slightly.

Calculations were performed using model (3), for a roughness of $\delta X = 1.5$ nm and a correlation length $L = 50$ and 100 nm, and for a roughness of $\delta X = 3$ nm and a correlation length $L = 100$ nm. In all cases no other roughness was included in the calculations. The results are shown in figure 3. There are no abrupt steps in the apparent resolution, only small oscillations at depths smaller than 50 nm as in model (2). For very small values of the correlation length, however, the roughness saturation value is reached very quickly, and this would be seen as either a steep increase in the first few nanometres or even as a larger apparent energy resolution starting at the very surface.

For the same value of δX, the same saturation roughness is always attained. This means that, after a certain depth, spectra with the same δX will look exactly the same, independently of their correlation lengths. However, at depths corresponding to a path length smaller than around the largest of the correlation lengths involved, the spectra look different. For the cases calculated the largest correlation length involved is 100 nm, which for an angle $\vartheta = 10^\circ$ corresponds to a depth of 17.4 nm; that is, about the first two bilayers. Indeed, the spectra calculated for $\delta X = 1.5$ nm and $L = 50$ and 100 nm become very similar at the third Ge peak, and equal in the fourth and fifth Ge peaks. On the other hand, for correlation lengths larger than about 35 nm, which at $\vartheta = 10^\circ$ corresponds to the path length in the first Ge layer, the first Ge peak is almost unchanged by the roughness, as the broadening due to roughness is still very small in that region.

3.4. Calculations: effect of angle of incidence

Calculations of the dependence of the roughness broadening with the angle of incidence are presented in figure 4 for all three models.

At non-grazing angles of incidence, the influence of roughness at small depths is very small for models (2) and (3). For these two models the effect of roughness depends on the path length of the beam inside the sample (for model (3) this is true only until the saturation roughness has been reached); the path length of the beam inside each layer increases with $1/\sin\vartheta$, amplifying the effect of roughness for grazing angles

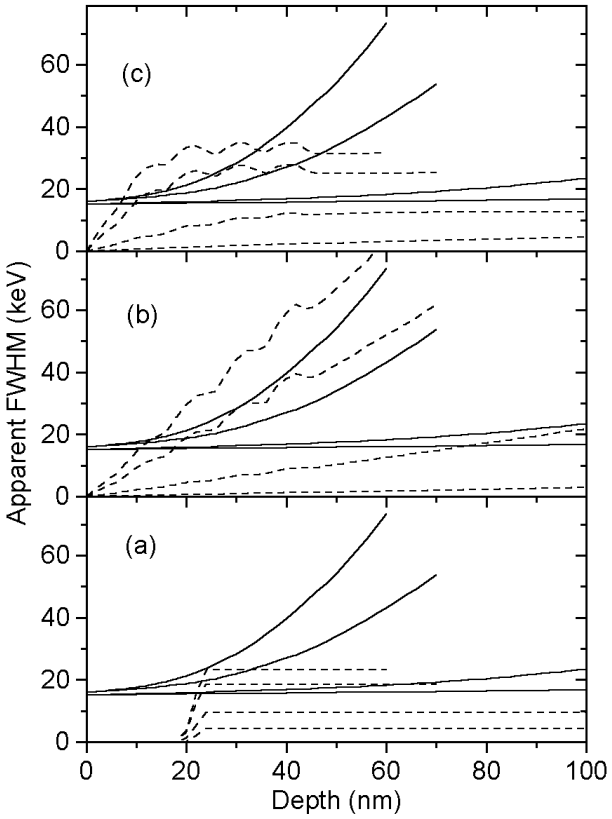

Figure 4. Calculations for system Si/(Si 4 nm/Ge 6 nm)$_5$ with roughness models (a) (1) $\delta X = 2$ nm at the third Ge layer; (b) (2) $\delta\vartheta = 1^\circ$; and (c) (3) $\delta X = 3$ nm, $L = 100$ nm. Dashed curves, contribution due to roughness. Full curves, contribution due to system resolution and energy straggling. The total apparent FWHM is the result of adding the two contributions in quadrature. The angles of incidence are $\vartheta = 50^\circ, 20^\circ, 10^\circ, 8^\circ$. Higher values of the apparent FWHM correspond to lower (more grazing) values of ϑ.

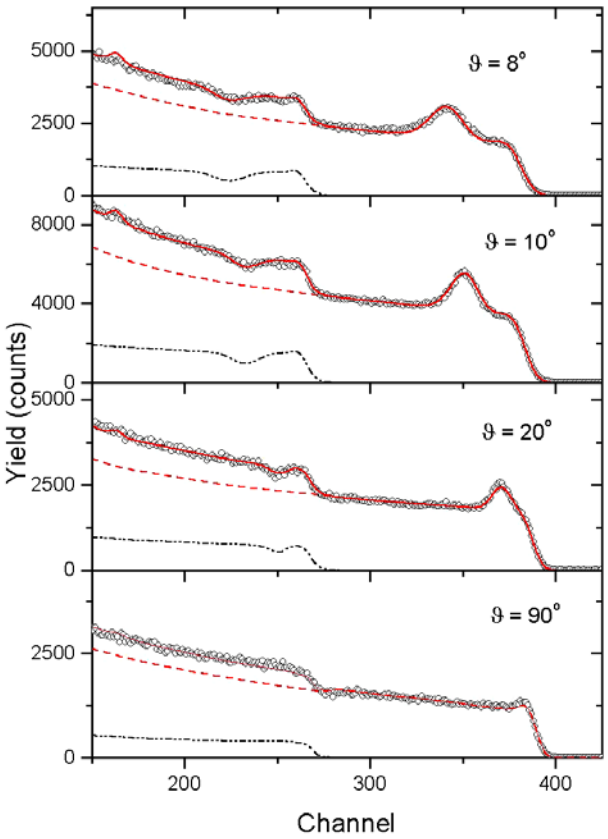

Figure 5. Fits (full curves) and data (circles) obtained for the sample Si/VS/$Si_{0.65}Ge_{0.35}$300nm/$Si_{0.2}Ge_{0.8}$4nm/$Si_{0.65}Ge_{0.35}$ 15 nm/Si 3 nm.

and making it very small otherwise. For model (1), the roughness is given for one (or more) well defined layer, and hence the full broadening due to roughness is felt as soon as the beam passes through that layer.

One should further note that the contribution to *depth* resolution due to roughness does not depend on the angle of incidence in model (1); it is always given by equation (1), which has no dependence on ϑ. However, the corresponding contribution to energy resolution does depend on ϑ, because through equation (2) it depends on the stopping cross section [ε], which depends strongly on the angle of incidence. This dependence of the energy resolution on the angle of incidence due to the stopping cross section is also present in models (2) and (3), but to it one must add the direct dependence as given in equations (3) and (4).

Summarizing, it is clear that the dependence of the apparent energy resolution on the angle of incidence depends on the roughness model considered. In all models there is a dependence due to the stopping cross section; in model (2) an extra dependence on tg ϑ exists; and in model (3) there is also an extra dependence, but with the form erf(a tgϑ). Hence, it is, in principle, possible to distinguish between the models by measuring a given sample at different angles of incidence.

4. Applications

4.1. Si/SiGe systems

Si–$Si_{1-x}Ge_x$ quantum wells have possible applications in optoelectronics with potential for monolithic integration with Si technology [27, 28]. The layer quality and interface sharpness have a strong influence on the optical properties of Si/SiGe systems [29].

A Si/VS/$Si_{0.65}Ge_{0.35}$300nm/$Si_{0.2}Ge_{0.8}$ 4 nm/$Si_{0.65}Ge_{0.35}$ 15 nm/Si 3 nm thin film, where VS stands for a linearly composition-graded virtual substrate, was studied by RBS. The nominal thickness of the $Si_{0.2}Ge_{0.8}$ channel was confirmed to be 4 nm by transmission-electron microscopy (TEM) [30]. Furthermore, the TEM results showed the channel layer and the top $Si_{0.65}Ge_{0.35}$ 15 nm layer to have an inhomogeneity in the thickness with an average height of 1.3 nm and correlation length $L = 43$ nm. Given this knowledge it is not necessary to test models (2) and (3), and the analysis can be made using only model (1).

The simultaneous fit obtained for all the angles of incidence measured is shown in figure 5. All the spectra are well reproduced. The stoichiometry of the channel layer was kept constant at the nominal value, because, to a certain extent, the exact Ge concentration and the amount of roughness can compensate for each other. The layer structure fitted is given in table 1. The amount of Si in the surface oxide and in the pure Si layer corresponds to 2.5 nm, close to the nominal 3 nm Si which does not take natural oxidation into account. The

Table 1. Nominal and fitted layer structure for a Si/SiGe structure. Thickness values were calculated assuming weighted averages of the densities of Si and Ge.

Layer	Nominal	Fitted
0	—	SiO_2 2.6 nm
1	Si 3 nm	Si 1.4 nm
2	$Si_{0.65}Ge_{0.35}$ 15 nm	$Si_{0.67}Ge_{0.33}$ 14.3 nm, $\delta X = 2.4$ nm
3[a]	$Si_{0.2}Ge_{0.8}$ 4 nm	$Si_{0.2}Ge_{0.8}$ 4.6 nm, $\delta X = 2.3$ nm
4	$Si_{0.65}Ge_{0.35}$ 300 nm	$Si_{0.65}Ge_{0.35}$ 312 nm
5[b]	VS	VS

[a] Stoichiometry kept constant in the fit.
[b] Not fitted.

fitted thickness and composition of the other layers are in close agreement with the nominal values.

In particular, the fitted thickness of the channel was 4.6 nm, which is very close to the 4.0(5) nm determined by TEM. As the area of the Ge channel peaks is a measure of the total amount of Ge in the channel, this is a clear indication that the Ge concentration in the channel cannot be too far from 80 at.%; if it were much larger, the thickness obtained would be much smaller, and if it were much smaller, the thickness obtained would be much larger, in disagreement with the TEM results. If anything, the Ge concentration can be slightly greater than 80 at%.

As for the values obtained for the layer thickness inhomogeneity, they are about 1 nm larger than the TEM values. This can have different causes. One of them is the error in the DEPTH calculation. As pointed out in section 3.1, if the energy straggling is underestimated, the value calculated will not be enough to fully account for the observed broadening of the signal measured, which will then be assigned to an artificial layer roughness. Another source of error, however, is that the region of the sample which is probed is very small, a few micrometres at most, while the RBS analysing beam is macroscopic. For the conditions of analysis, the beam spot at $\vartheta = 8^\circ$ is 0.6×1.4 mm^2. Hence the scales probed are very different, and the roughness measured with TEM may be a local value only.

Nevertheless, the values obtained with the RBS roughness model developed are at the very least of the correct order of magnitude. Furthermore, a data analysis that would have ignored the effect of roughness would have led to completely wrong values for the thickness and stoichiometry of the channel layer, which determine the properties of these systems.

4.2. Fe/Co multilayers

A MgO/(Fe 23 Å/Co 20 Å)$_{10}$/C 60 Å sample was analysed by RBS at $\vartheta = 45^\circ$ and $\vartheta = 10^\circ$. Fe and Co are miscible, and the occurrence of interfacial mixing was expected. This has been confirmed using perturbed angular correlations (PAC) on similar samples grown on GaAs, which indicated that around 75% of the sample consisted of a diffuse interface [31].

The spectra obtained are shown in figure 6. A simulation assuming that no interfacial mixing is present leads to a very large misfit. As was noted in section 3.2 in point (4), a multilayer where there is interfacial mixing between layers can be modelled using model (3) with a correlation length about as large as the thickness of the first bilayer. We hence fitted

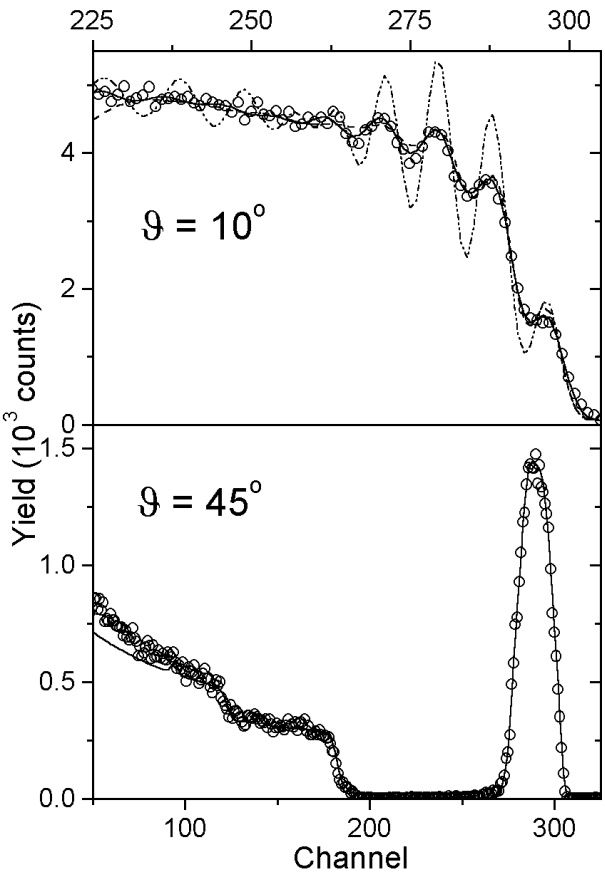

Figure 6. Fits (full curves) and data (circles) obtained for the sample MgO/(Fe 23 Å/Co 20 Å)$_{10}$, with model (3). The fit obtained with model (2) (dashed curves) and a simulation made assuming no interfacial mixing (dash–dot–dotted curve) are also shown for $\vartheta = 10^\circ$.

the data with model (3), which led to a very small value of the correlation length $L = 9.4$ nm, which is about the same as the sum of the thickness of the first Fe/Co bilayer with the top C layer, totalling 10 nm.

The fitted standard deviation was 1.4 nm (corresponding to a FWHM of 3.3 nm, which can be taken as the interface thickness) for a bilayer thickness of 4.3 nm; that is, only about 1.1 nm of pure Fe and Co would remain. A manual fit to the data assuming a MgO/(Fe t_{Fe}/FeCo t_{int}/Co t_{Co}/FeCo t_{int})$_9$/Fe t_{Fe}/FeCo t_{int}/Co t_{Co}/C 60 Å structure led to $t_{Fe} = 0.5$ nm, $t_{Co} = 0.8$ nm, and $t_{int} = 3.0$ nm, which, being in excellent agreement with the results using the roughness models, is very difficult and time consuming to perform, and depends on visual comparisons which are to some extent subjective.

A fit with model (2) was also done and the results are also shown in figure 6. The fit obtained is worse than that using model (3), and correspondingly the χ^2 obtained is larger, 8.3 as compared to 6.0 for model (3). This is a consequence of the fact that model (2) leads to an increase of the broadening for $\vartheta = 10^\circ$ that is faster than that observed: in model (3) there is a rapid increase in the broadening due to roughness in the first bilayer, and a constant value after that. In contrast, in model (2) the broadening due to roughness increases linearly with depth.

5. Summary

Data analysis of RBS and other IBA techniques has, in most cases, been performed without considering the effect of layer roughness in the data. This has been due to difficulties of modelling roughness and of coding the models developed in standard analysis programs. The approaches so far presented have been, in some cases, less than satisfactory, in other cases developed for particular problems and/or systems, and in still other cases the resulting necessary calculations are cumbersome and long, as they involve calculating many (from a few to thousands) spectra for different surface entry points.

In this work, a new approach was proposed and developed: the effect of roughness is, in many cases, similar to that of energy straggling, that is, it leads to additional broadening of any spectral feature. By calculating the broadening due to a certain kind of roughness and assigning it as an extra contribution to the energy straggling, an apparent energy resolution is obtained which can be convoluted with the theoretical spectrum in the normal way. The effect of roughness can thus be included in a standard code with little effort, paying only a small price in terms of calculation time.

The code developed will not work correctly in cases where the surface roughness is so large that the beam comes in and out of the sample more than once. This effect has been experimentally observed in the past in some very few cases, and there are codes developed specifically to analyse it. Nevertheless, the algorithms implemented in this paper are useful in the majority of cases found in systems normally studied with RBS.

Finally, the code was also implemented for ERDA, however, lacking data, it still has not been tested for that experimental technique.

Acknowledgments

I would like to thank Dr Edit Szilágyi for many useful discussions on energy straggling, Drs Paulo de Freitas, J Dekoster and Oleg Mironov for providing the samples, Dr Maria Fernanda da Silva and Professor José Carvalho Soares for access to the high-resolution RBS facility, Dr Chris Jeynes for reading the manuscript, and A Wartig for the pictures. The support of the Fundação para a Ciência e Tecnologia is gratefully acknowledged.

References

[1] Tesmer J R and Nastasi M (eds) 1995 *Handbook of Modern Ion Beam Materials Analysis* (Pittsburgh, PA: Materials Research Society)
[2] Bird J R, Duerden P, Cohen D D, Smith G B and Hillery P 1983 *Nucl. Instrum. Methods* **218** 53
[3] Tavares C J, Rebouta L, Alves E J, Almeida B, Bessa e Sousa J, da Silva M F and Soares J C 1998 *Nucl. Instrum. Methods* B **136–138** 278
[4] Barradas N P, Soares J C, da Silva M F, Pászti F and Szilágyi E 1994 *Nucl. Instrum. Methods* B **94** 266
[5] Niwa H, Nakao S and Saitoh K 1998 *Nucl. Instrum. Methods* B **136–138** 297
[6] Elliman R G, Timmers H, Palmer G R and Ophel T R 1998 *Nucl. Instrum. Methods* B **136–138** 649
[7] Rissanen L, Dahr S, Lieb K P, Engel K and Wenderoth M 2000 *Nucl. Instrum. Methods* B **161–163** 986
[8] Edge R D and Bill U 1980 *Nucl. Instrum. Methods* **168** 157
[9] Knudson A R 1980 *Nucl. Instrum. Methods* **168** 163
[10] Hobbs C P, McMillan J W and Palmer D W 1988 *Nucl. Instrum. Methods* B **30** 342
[11] Shorin V S and Sosnin A N 1992 *Nucl. Instrum. Methods* B **72** 452
[12] Itoh Y, Maeda T, Nakajima T, Kitamura A, Ogiwara N and Saidoh M 1996 *Nucl. Instrum. Methods* B **117** 161
[13] Yesil I M, Assmann W, Huber H and Löbner K E G 1998 *Nucl. Instrum. Methods* B **136–138** 623
[14] Behrisch R, Grigull S, Kreissig U and Grötzschel R 1998 *Nucl. Instrum. Methods* B **136–138** 628
[15] Barradas N P, Jeynes C and Webb R P 1997 *Appl. Phys. Lett.* **71** 291
[16] Barradas N P, Jeynes C, Webb R P, Kreissig U and Grötzschel R 1999 *Nucl. Instrum. Methods* B **149** 233
[17] Barradas N P and Smith R 1999 *J. Phys. D: Appl. Phys.* **32** 2964
[18] Pászti F, Manuaba A, Hadju C, Melo A A and da Silva M F 1990 *Nucl. Instrum. Methods* B **47** 187
[19] Yang Q, O'Connor D J and Wang Z 1991 *Nucl. Instrum. Methods* B **61** 149
[20] Szilágyi E, Pászti F and Amsel G 1995 *Nucl. Instrum. Methods* B **100** 103
[21] Szilágyi E 2000 *Nucl. Instrum. Methods* B **161–163** 37
[22] Szilágyi E and Pászti F 1994 *Nucl. Instrum. Methods* B **85** 616
[23] Barradas N P, Jeynes C, Mironov O A, Phillips P J and Parker E H C 1998 *Nucl. Instrum. Methods* B **139 239–243**
[24] Ziegler J F, Biersack J P and Littmark U 1985 *Stopping and Ranges of Ions in Solids* (New York: Pergamon)
[25] Chu W-K, Mayer J W and Nicolet M-A 1978 *Backscattering Spectrometry* (Orlando, FL: Academic) p 77–9
[26] Kotái E 1994 *Nucl. Instrum. Methods* B **85** 588
[27] Karunasiri R P G, Park J S and Lang K L 1991 *Appl. Phys. Lett.* **59** 2588
[28] Robins D J, Standway M B, Leong W Y, Glasper J L and Pickering C 1995 *J. Mater. Sci: Mater. Electron.* **6** 353
[29] Mironov O A *et al* 1997 *Thin Solid Films* **306** 307
[30] Myronov M, Mironov O A, Phillips P J, Parker E H C, Barradas N P, Franco N, Sequeira A D and Alves E 2001 *Proc. E-MRS 2001 Spring Meeting Symposium D: 2nd Int. Conf. Silicon Epitaxy and Heterostructures* submitted
[31] Swinnen B 1997 Structure and interfacial magnetism of Fe/Co Multilayers *PhD Dissertation* Katholieke Universiteit Leuven pp 79–80